Density Functional Study of H-Induced Defects as Nucleation Sites in Hybrid Carbon Nanomaterials

A. S. Barnard,*,† M. L. Terranova,‡ and M. Rossi§,||

Center for Nanoscale Materials, Argonne National Laboratory, 9700 South Cass Avenue, Argonne, Illinois, 60615, Dip. Scienze e Tecnologie Chimiche, Un. "Tor Vergata", Via della Ricerca Scientifica, 00133, Roma, Italy, and Dip. di Energetica and INFM, Un. "La Sapienza", Via A. Scarpa 14, 00161 Roma, Italy

Received July 12, 2004. Revised Manuscript Received October 18, 2004

Recently we have reported on the growth of an exciting new class of hybrid nanostructured carbon materials, coupling nanosized diamond with single-walled carbon nanotubes. The inner structures were shown to be single-walled C nanotubes or bundles of single-walled nanotubes up to 15 μm long, and the outer deposit consisted of faceted diamond crystallites with diameters in the range of 20−100 nm. To aid in understanding the mechanisms responsible for the formation of such materials, the present study uses density functional theory to examine the role of atomic hydrogen in creating localized sp^3 hybridized defects on the outer wall of carbon nanotubes. The results illustrate that certain absorption configurations may produce defects containing dangling carbon bonds, and thus promote the formation of suitable sites for nanodiamond nucleation.

1. Introduction

Recent decades have seen great advances in the field of nanoscience and nanotechnology. Beyond nanoparticles, nanotubes, or nanowires, the next generation of nanomaterials are expected to be more complicated architectures and hybrid structures with controllable structural, electronic, and chemical properties. Such materials must be robust, reliable, and constructed from readily accessible components that may be engineered to form desired shapes. The well-documented differences in the thermal, mechanical, and electronic properties of the various allotropes of carbon,[1] along with their chemical compatibility, make hybrid nanomaterials that couple nanotubes and nanodiamond an attractive prospect. Currently there are two main synthesis routes in this direction, either the consecutive growth or fabrication of respective phases to form one nanostructure, or the controlled, partial transformation of one phase of nanocarbon into another.

The latter has to some degree already been realized. Experimentally, it has been found that upon annealing (1200−1800 K) 2−5-nm nanodiamond particles transform into carbon-onions.[2] Further, the reverse transition of carbon-onions to nanocrystalline diamond under electron irradiation has been observed.[3] These transformations have also been modeled using various levels of theory.[4−8] Similarly, carbon nanotubes (CNTs) have also been shown to transform to nanodiamond under different experimental conditions.[9−14] Here, although not fully understood, the transformation progression was proposed to nanodiamond,[15] again involving a phase transition between sp^2 and sp^3 bonded quasi-zero dimensional carbon nanoparticles.

However, rarely does a complete nanodiamond or carbon-onion result from such transitions. Usually an intermediary is formed with a diamond-like core and an onion-like outer shell of varying thickness. Studies concerning these intermediaries, both X-ray absorption and emission measurements on nanodiamonds synthesized in detonation waves from high explosives and theoretical simulations, have suggested that a new class of carbon (so-called "bucky-diamonds") be established to describe them.[16] Although bucky-diamonds may be thought of as hybrid carbon nanoparticles (with a core−shell structure), they are not traditionally considered

* To whom correspondence should be addressed. E-mail: amanda.barnard@anl.gov.
† Argonne National Laboratory.
‡ Dip. Scienze e Tecnologie Chimiche, Un. "Tor Vergata", Via della Ricerca Scientifica. E-mail: terranova@roma2.infn.it.
§ Dip. di Energetica and INFM, Un. "La Sapienza". E-mail: marcorossi@uniroma1.it.
|| Present affiliation: Dip. di Energetica, Un. "La. Sapeinza", Via A. Scarpa 14, 00161 Roma, Italy.

(1) Shenderova, O. A.; Zhirnov, V. V.; Brenner, D. W. *Crit. Rev. Solid State Mater. Sci.* **2002**, *27*, 227.
(2) Kuznetsov, V. L.; Chuvilin, A. L.; Butenko, Y. V.; Mal′Kov, I. Y.; Titov, V. M. *Chem. Phys. Lett.* **1994**, *209*, 72.
(3) Banhart, F.; Ajayan, P. M. *Nature* **1996**, *382*, 433.
(4) Winter, N. W.; Ree, F. H. *J. Comput.-Aided Mater. Des.* **1998**, *5*, 279.
(5) Kuznetsov, V. L.; Zilberberg, I. L.; Butenko, Y. V.; Chuvilin, A. L.; Seagall, B. *J. Appl. Phys.* **1999**, *86*, 863.
(6) Fugaciu, F.; Hermann, H.; Seifert, G. *Phys. Rev. B* **1999**, *60*, 10711.
(7) Barnard, A. S.; Russo, S. P.; Snook, I. K. *Philos. Mag. Lett.* **2003**, *83*, 39. Barnard, A. S.; Russo, S. P.; Snook, I. K. *Diamond Relat. Mater.* **2003**, *12*, 1867.
(8) Astala, R.; Kaukonen, M.; Jungnickel, G.; Frauenheim, Th.; Nieminen, R. M. *Phys. Rev. B* **2001**, *63*, 81402.
(9) Wei, B. Q.; Zhang, J. H.; Liang, J.; Gao, Z. D.; Wu, D. H. *J. Mater. Sci. Lett.* **1997**, *16*, 402.
(10) Wei, B. Q.; Liang, J.; Gao, Z. D.; Zhang, J. H.; Zhu, Y. Q.; Li, Y. B.; Wu, D. H. *J. Mater. Process. Technol.* **1997**, *63*, 573.
(11) Zhu, Y. Q.; Sekine, T.; Kobayashi, T.; Takazawa, T.; Terrones, M.; Terrones, H. *Chem. Phys. Lett.* **1998**, *287*, 689.
(12) Cao, L. M.; Gao, C. X.; Sun, H. P.; Zou, G. T.; Zhang, Z.; Zhang, X. Y.; He, M.; Zhang, M.; Li, Y. C.; Zhang, J.; Dai, D. Y.; Sun, L. L.; Wang, W. K. *Carbon* **2001**, *39*, 287.
(13) Hou, Y. Q.; Zhuang, D. M.; Zhang, G.; Wu, M. S.; Liu, J. J. *Appl. Surf. Sci.* **2002**, *185*, 303.
(14) Yusa, H. *Diamond Relat. Mater.* **2002**, *11*, 87.
(15) Wei, B.; Zhang, J.; Liang, J.; Wu, D. *Carbon* **1998**, *36*, 997.
(16) Raty, J. Y.; Galli, G.; Bostedt, C.; Buuren, T. W.; Terminello, L. J. *Phys. Rev. Lett.* **2003**, *90*, 37402.

10.1021/cm0488682 CCC: $30.25
Published on Web 01/14/2005

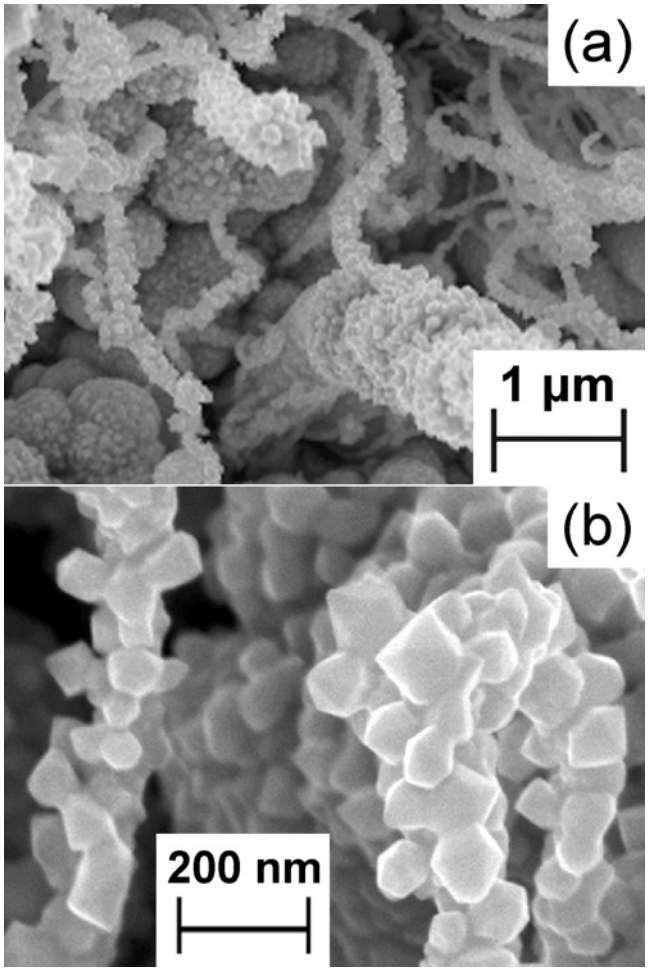

Figure 1. Two FE-SEM images showing SWNT nanotubes and bundles of SWNT covered by nanodiamonds (a), with a more detailed image showing the faceted shape of the individual nanocrystals (b).

in this way and so far little advantage has been taken from the dual-phase nature of these nanomaterials.

Alternatively, hybrid nanocarbon materials have also been formed via the successive growth of one phase (usually nanodiamond) onto a preexisting nanomaterial of a complementary phase. Recently Rossi et al[17] have described the successful growth of uniform nanocrystalline diamond coatings onto commercial vapor grown carbon fibers. The coatings had a grain size of 5−50 nm and an intermediate layer of turbostratic graphite was identified at the film/fiber interface.[17] Following from this result, Terranova et al[18] have reported on the growth and characterization of hybrid nanocarbon systems, coupling nanodiamond and carbon nanotubes as shown in Figure 1. The nanodiamonds (with diameters in the range 20−100 nm) have been nucleated and grown directly on single-walled nanotubes (SWNTs), and bundles of SWNTs up to 15 μm long, in a modified CVD reactor by means of reactions between carbon nanopowders and atomic H.[18] A time−growth sequence for the two carbon nanophases has been outlined, along with details of the one-step synthesis approach that provides an experimental route to the production of ordered arrays of rigid hybrid nanocarbon structures.[18]

In contrast, Sun et al[19] observed the degradation of multiwalled carbon nanotubes into amorphous carbon nanorods before the hydrogen plasma induced transformation into nanocrystalline diamond was observed. The authors prepared groups of pure CNTs and carbon ion beam irradiated CNT samples (approximately 20−40 nm in diameter and consisting of 20−30 concentric shells) that were postprocessed by heating in the PECVD reaction chamber in the presence of hydrogen. After irradiation the nanotubes were found to evolve into amorphous carbon nanorods, with uniform diameters and a smooth longitudinal surface. After reaction for several hours, the vacuum-cooled specimens showed defective sites on both the inner and outer walls of CNTs, and the formation of nearly spherical amorphous carbon clusters. With the increase in treatment time, nanodiamond particles were observed as well as a rapid increase in particle density.[19]

The aim of the present work has been to assist in the identification of the mechanisms responsible for formation of these structures, with special attention given to the initial stages of nucleation. Following a summary of the current knowledge in this area, the results of ab initio methods examining the development of suitable nucleation sites on the outer walls of SWNTs are presented.

2. Proposed Mechanisms

It has been proposed that defects on the outer walls of CNTs are the origin of the nucleation (and subsequent growth) of diamond nanoparticles by hydrogen plasma treatment.[18,19] Such defects, characterized by a finite region of sp^3 bonded C atoms in an otherwise sp^2 bonded material, may be formed as a result of chemisorption of individual H atoms.

In an experimental study of the interaction of atomic hydrogen with various forms of sp^2 bonded carbon (fullerenes, SWNTs, and planar graphene) Ruffieux et al[20] found that the energy barrier for hydrogen adsorption decreases with increasing local curvature. This implies not only that hydrogen chemisorption (and the subsequent re-hybridization from sp^2 to sp^3) will be easier on the curved walls of carbon nanotubes than planar graphene, but also that the probability of H adsorption in a suitable plasma will increase with decreasing CNT radius of curvature.[21] In addition to atomic H adsorption (as mentioned above), Sun et al have also treated CNTs in a H_2 atmosphere, and have annealed CNTs in a vacuum.[19] In both cases, no changes were reported in the structure of the CNTs, thereby demonstrating that *atomic* hydrogen is essential in the formation of suitable defect sites, in agreement with the results of Ruffieux.[20]

Therefore, if each C−H bond resulting from individual H adsorbates is considered as an isolated point defect on the

(17) Rossi, M.; Terranova, M. L.; Piccirillo, S.; Sessa, V.; Manno, D. *Chem. Phys. Lett.* **2005**, in press.
(18) Terranova, M. L.; Orlanducci, S.; Fiori, A.; Tamburri, E.; Sessa, V.; Rossi, M.; Barnard, A. S. *Chem. Mater.* **2004**, submitted.
(19) Sun, L. T.; Gong, J. L.; Zhu, Z. Y.; Zhu, D. Z.; He, S. X.; Wang, Z. X.; Chen, Y.; Hu, G. *Appl. Phys. Lett.* **2004**, *84*, 2901.
(20) Ruffieux, P.; Gröning, O.; Bielmann, M.; Mauron, P.; Schlapbach, L.; Gröning, P. *Phys. Rev. B* **2002**, *66*, 245416.
(21) Ruffieux, P.; Gröning, O.; Bielmann, M.; Gröning, P. *Appl. Phys. A* **2004**, *78*, 975.

sp^2 network, the continued hydrogenation of the CNT walls will either result in clustering of sp^3 defects or it will increase the density of isolated sp^3-point defects. The former may result in the formation of finite-sized defect sites on an otherwise sp^2 bonded structure; and the latter (as the density increases) may eventually result in a structure with more homogeneously mixed hybridization such as amorphous carbon nanowires.

Once formed, sp^3 defects offer suitable sites for the nucleation of carbon nanoparticles. It is currently thought that the nuclei initially form an amorphous structure,[19] which then undergo a phase transition into the diamond structure (crystallization).[22] Crystallization will involve physical and chemical reactions including the formation and migration of hydrocarbons, hydrogen abstraction and the dehydrogenation of hydrocarbons absorbed on the surface of the forming nuclei. Following nucleation and crystallization the growth of diamond may proceed epitaxially, since the hydrogen plasma etching mediates the carbon atom displacement from amorphous phase to ordered diamond phase and prevents graphite formation.

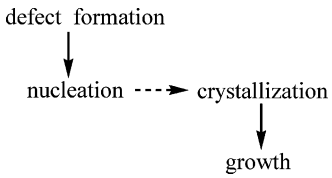

Therefore, it can been seen that this process is entirely dependent upon the creation of suitable sp^3 defects on the outer surface of the nanotubes, without which the necessary nucleation will not be able to proceed. In the present study the creation of local, finite defects by clustering of H adsorbates has been investigated as a function of adsorption geometry.

3. Ab initio Modeling of sp^3 Defect Formation

Working on the hypothesis that atomic hydrogen impinging on the wall of a SWNT creates sp^3 defects sites, we have undertaken first principles calculations to investigate the effects of atomic hydrogen adsorbates on the hybridization in model (6,6) and (9,0) SWNTs. The adsorption of hydrogen was simulated on the outer wall of the model SWNTs (exohedral), and (following full ionic and electronic relaxation) the final structures were characterized by examining the electronic charge density and constructing sp^2 isosurfaces.

The first principles calculations have been carried out using density functional theory (DFT) within the generalized-gradient approximation (GGA), with the exchange-correlation functional of Perdew and Wang (PW91).[23] This has been implemented via the Vienna ab initio simulation package (VASP),[24,25] which spans reciprocal space with a plane-wave basis. All calculations were performed with the valence orbitals expanded in a plane-wave basis up to a kinetic energy of 290 eV. The linear tetrahedron method (with Blöchl corrections) was used for the Brillouin zone integrations, with $4 \times 4 \times 4$ Monkhorst−Pack[26] k-point mesh. Although this choice of k-mesh results in superfluous k-points in the nonperiodic directions, it was found that the inclusion of these k-points is more consistent with the LTM.

We have used a relaxation technique involving an efficient matrix-diagonalization routine based on a sequential band-by-band residual minimization method of single-electron energies,[27,28] with direct inversion in the iterative subspace. During the relaxations we used ultra-soft, gradient-corrected Vanderbilt-type pseudopotentials (US−PP)[29,30] and real-space projected wave function character (to decrease the computational cost), and relaxed to a total energy convergence of 10^{-4} eV. The following (final) calculations of the electronic charge density (ECD) were then performed using the projected augmented wave (PAW) potentials,[31] with a basis set increased by 30% and reciprocal-space projected wave function character (to improve accuracy), also to a convergence of 10^{-4} eV. PAW potentials are generally considered to be more accurate than the ultra-soft pseudopotentials,[32] since the radial cutoffs (core radii) are smaller than the radii used for the US pseudopotentials, and the fact that the PAW potentials reconstruct the exact valence wave function with all nodes in the core region.

3.1 Hydrogen-Induced Distortions in the Nanotube Structure. Initially, changes in the structure were examined for the single walled (6,6) and (9,0) nanotubes with 144 and 108 atoms in the (periodic) simulation cell respectively; and one, two, and three hydrogen atoms chemisorbed onto the outer side of each tube wall. Multiple hydrogen atoms were adsorbed onto carbon atoms which were second-nearest-neighbors with respect to one another, thereby forming clusters of C−H bonds akin to the structure of a C(111):H surface of diamond. In the cases where three hydrogen atoms were absorbed, two different configurations were examined. The first configuration involved the adsorption of the hydrogen atoms equidistant around one of the six-membered rings in the tube wall (ring-configuration). The second configuration involved the adsorption of hydrogen atoms around the base of a triangular pyramid, formed by three carbon atoms bound to the same carbon in the center (pyramid-configuration). Diagrams of these configurations are shown in the top and bottom panels of Figure 2, respectively.

The effects of H adsorption upon the structure of the SWNTs are shown in Figures 3 and 4 for the (6,6) and (9,0) nanotubes, respectively. It was found that the overall cylindrical shape of the (6,6) nanotubes was perturbed very little by the addition of the hydrogen atoms. The (9,0) nanotube however, showed more significant distortion when more than two hydrogen atoms were adsorbed. As indicated

(22) Fyta, M. G.; Remediakis, I. N.; Kelires, P. C. *Phys. Rev. B* **2003**, *67*, 035423.
(23) Perdew, J.; Wang, Y. *Phys. Rev. B* **1992**, *45*, 13244.
(24) Kresse, G.; Hafner, J. *Phys. Rev. B* **1993**, *47*, R558.
(25) Kresse, G.; Hafner, J. *Phys. Rev. B* **1996**, *54*, 11169.
(26) Monkhorst, H. J.; Pack, J. D. *Phys. Rev. B* **1976**, *13*, 5188.
(27) Kresse, G.; Furthmüller, J. *Comput. Mater. Sci.* **1996**, *6*, 15.
(28) Wood, D. M.; Zunger, A. *J. Phys. A* **1985**, *18*, 1343.
(29) Vanderbilt, D. *Phys. Rev. B* **1990**, *41*, 7892.
(30) Kresse, G.; Hafner, J. *J. Phys.: Condens. Matter* **1994**, *6*, 8245.
(31) Blöchl, P. E. *Phys. Rev. B* **1994**, *50*, 17953.
(32) Kresse, G.; Joubert, J. *Phys. Rev. B* **1999**, *59*, 1758.

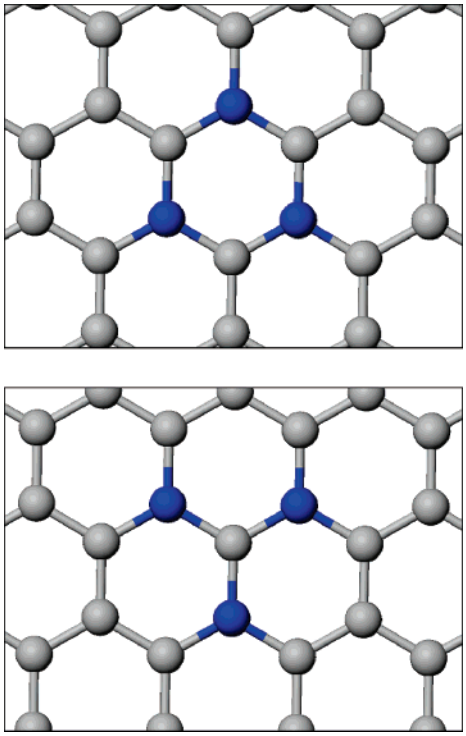

Figure 2. Two adsorption configurations for three hydrogen atoms on the outer walls of the SWNT indicated by the carbon atoms shown in dark blue. The three H atoms in the so-called "ring-configuration" (top) are adsorbed equidistant around a six-membered ring, and the three H atoms in the "pyramid-configuration" (bottom) are adsorbed around the base of a triangular pyramid.

in Figure 4, the (9,0) nanotube has adopted a slightly "egg"-shaped cross section and some buckling in the structure of the wall around the C−H bonds. This distortion is more pronounced when the H atoms are adsorbed in the ring-configuration (Figure 4c) than in the pyramid-configuration (Figure 4d).

In each case, the structural and energetic changes have been listed in Table 1. Here, the average C−C bond lengths surrounding the C−H bonds are given (along with the average C−H bond length) as a function of the number of adsorbed H atoms and the adsorption configuration. Note that the C−C bonds in the region immediately surrounding the adsorbates are longer than the 1.42 Å of the sp^2 bonds of the remaining nanotube, and that this change decreases slightly with the number of adsorbed hydrogens. The alteration of the C−C bond lengths is accompanied by a protrusion distance, h, corresponding to the displacement of the C atoms (participating in the C−H bonds) outward from the ideal cylindrical plane of the clean nanotube. The same nomenclature was employed by Ruffieux et al[21] to describe local curvature effects.

The bond angles (θ) listed in Table 1 refer to the average angle formed by the C atoms participating in the C−H bonds with two of it's nearest-neighbors. The larger deviation of the angles of the C atoms in the nanotubes from the ideal graphitic 120 degrees concur with the larger protrusion distance of this structure. In general, the buckling characterized by the θ and h parameters is more significant in the (9,0) nanotube than in the (6,6) nanotube.

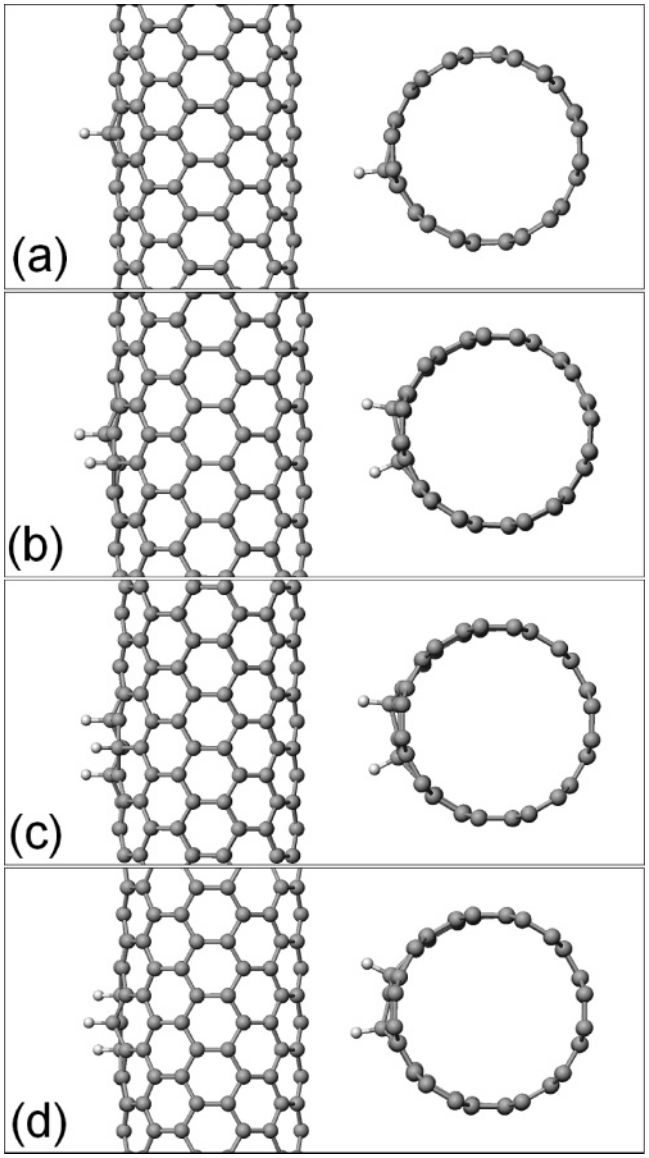

Figure 3. Views perpendicular (left) and parallel (right) to the principal axis of a (6,6) SWNT with 144 carbon atoms in the simulation cell, with (a) one, (b) two, and (c and d) three hydrogen atoms adsorbed to the outer wall. The three H atoms in (c) are adsorbed in the "ring-configuration, and the three H atoms in (d) are adsorbed in the "pyramid-configuration".

In addition to the examination of changes in structural parameters, the binding energy (E_b) was also calculated for each adsorption configuration, as defined by

$$E_b = (E_{CNT} + NE_H - E_{CNT,H_N})/N \qquad (1)$$

where E_{CNT} is the total energy of the clean nanotube, $E_{CNT,HN}$ is the total energy of the nanotube with H adsorbates, E_H is the energy of a hydrogen atom, and N is the number of adsorbed hydrogens. The results list in Table 1 shows that overall the binding energy was found to decrease with increasing number of hydrogens. Extrapolating this trend to a monolayer coverage the $E_b(\Theta = 1) = 2.73$ and 3.34 eV for the armchair and zigzag geometries, respectively. It is also important to note that for each degree (and configuration) of adsorption, E_b is lower for the nanotube with a larger diameter. Both of these observations are in agreement with

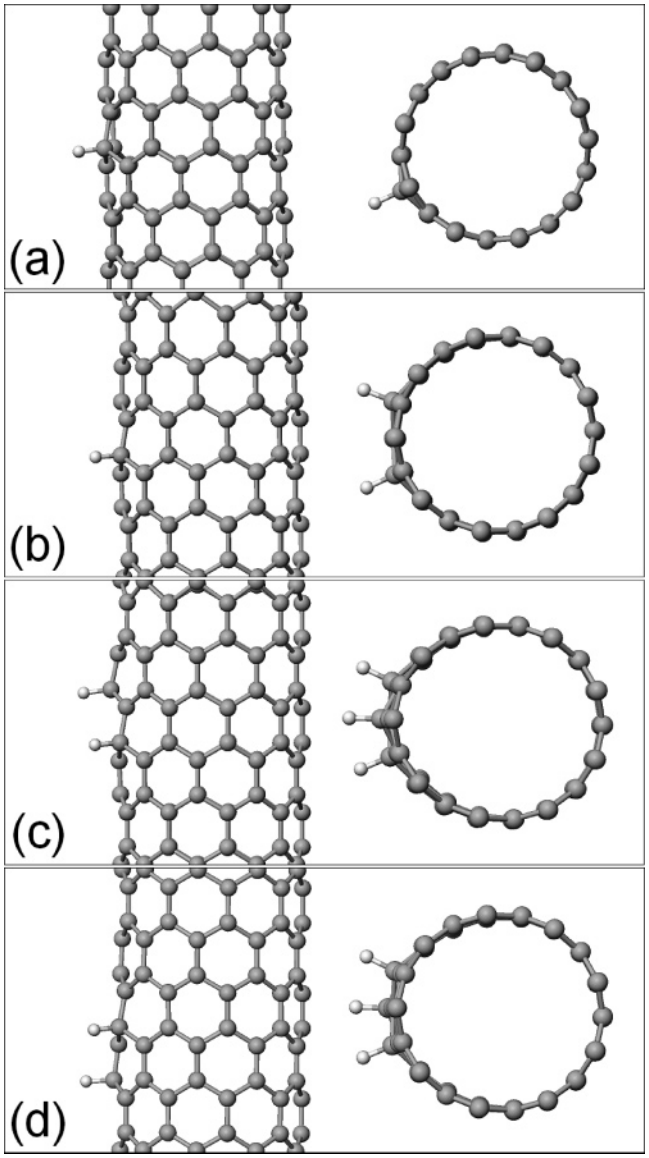

Figure 4. Views perpendicular (left) and parallel (right) to the principal axis of a (9,0) SWNT with 108 carbon atoms in the simulation cell, with (a) one, (b) two, and (c and d) three hydrogen atoms adsorbed to the outer wall. The three H atoms in (c) are adsorbed in the "ring-configuration", and the three H atoms in (d) are adsorbed in the "pyramid-configuration".

Table 1. Structural Distortions in the Region of the CNTs Localized about the H Adsorbates, Characterized by the Average C−C Bond Lengths, the Average C−H Bond Length and Protrusion Distance *h* (in Å), the Average Angle Formed by the C Atoms Surrounding the C−H Bond (in Degrees), and the H Binding Energy E_b as Defined in Equation 1 (in eV)

		1H	2H	3H − ring	3H − pyramid
C(6,6)	C−C	1.51	1.50	1.50	1.49
	C−H	1.11	1.11	1.12	1.12
	h	0.37	0.27	0.38	0.36
	θ	111.6	112.1	111.2	112.1
	E_b	3.60	3.47	3.42	3.38
C(9,0)	C−C	1.51	1.50	1.50	1.50
	C−H	1.11	1.12	1.12	1.12
	h	0.36	0.35	0.48	0.46
	θ	111.7	112.5	110.9	110.7
	E_b	3.69	3.65	3.63	3.58

the findings of Gülseren et al.[34] The most interesting aspect is, however, that when three hydrogen atoms are adsorbed together the pyramid-configuration is consistently lower in energy than the ring-configuration.

In general, distortions of the type outlined in Table 1 are expected to be representative of the changes in hybridization of the C−C bonds neighboring the C−H bonds of the adsorbed hydrogens. This was investigated by examining the ECD in the region of the distortions.

3.2 Electronic Charge Density and Changes in Hybridization. For the purposes of examining the bonding in the nanotubes, we have found that it is useful to generate 2-dimensional ECD profiles in a given plane of interest. Shown in Figure 5 are examples of the ECD in planes perpendicular and parallel to the axis of a (6,6) nanotube without any H atoms, along with a diagram showing the location of the planes. The ECD in the green plane perpendicular to the axis is shown to the left, and in the red plane parallel to the axis (and almost tangential to the nanotube wall) is shown to the right. In these ECD profiles the regions of high ECD (corresponding to sp^2 bonds) are colored red, and low ECD (corresponding to vacuum) are colored blue. In the following discussion, ECD profiles have been generated in planes parallel to the axis of the nanotubes, almost tangential wall (the red plane in Figure 5) so that changes in the charge distribution surrounding the C−H bonds may be highlighted.

Another useful (albeit semiquantitative) technique uses iso-surfaces to visualize the hybridization of the carbon bonds in the structure. By applying an iso-surface to the ECD at a fractional value of approximately 0.7 of the total, the localization of the ECD around the atoms is highlighted (in three dimensions), as shown in the left part of Figure 6. This represents the total bonding iso-surface for the nanotube. However, by applying an iso-surface to the ECD at a fractional value of approximately 0.9 of the total, an estimate can be made as to the location of sp^2 bonds in the structure[35] (right of Figure 6). In this example, as there are no hydrogen adsorbates, all of the bonds in the structure are sp^2 bonds (as expected). These sp^2 bonds appear as "dumb-bell" shaped surfaces between the atoms.[35] Note that C−H bonds are not shown in the following analysis.

The distribution of sp^2 bonds was found to change when hydrogen was adsorbed on the wall of the nanotubes. In the case of the (6,6) nanotube (shown in Figure 7), the ECD in the plane of interest illustrates the changes in the distribution of change surrounding the C−H bonds of the adsorbates. In addition to this, the corresponding iso-surfaces show evidence of changes in hybridization. As these are sp^2 iso-surfaces, the missing dumb-bell shaped bonds between carbon atoms indicate the existence of sp^3 bonds.[35] Similarly, the distribution of sp^2 bonds was found to change when hydrogen was adsorbed on the wall of the (9,0) nanotube (as shown in Figure 8). The ECD in the plane of interest also shows changes in the distribution of change surrounding the C−H bonds, and the corresponding iso-surfaces show evidence of sp^3 bonds surrounding the adsorbates.

(33) Becke, A. D.; Edgecombe, K. E. *J. Chem. Phys.* **1990**, *92*, 5397.
(34) Gülseren, O.; Yildirim, T.; Ciraci, S. *Phys. Rev. B* **2002**, *66*, R121401.
(35) This technique has been used extensively to examine the changes in hybridization of carbon atoms on the surfaces of nanodiamonds and diamond nanowires following surface delamination. See for example: Barnard, A. S.; Russo, S. P.; Snook, I. K. *Int. J. Mod. Phys. B* **2003**, *17*, 3865. Barnard, A. S.; Russo, S. P.; Snook, I. K. *J. Nanosci. Nanotechnol.* **2004**, *4*, 151.

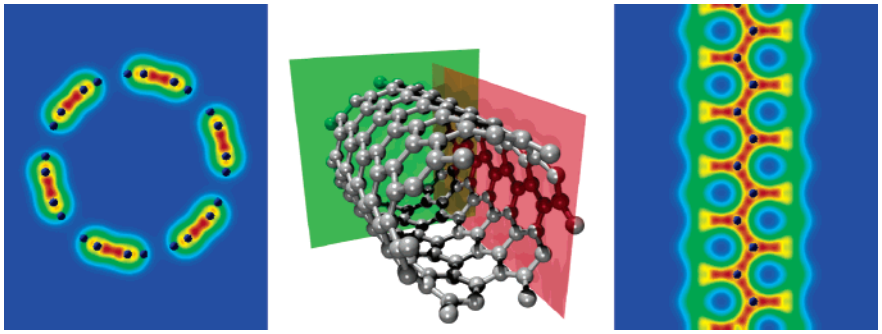

Figure 5. ECD for a (6,6) nanotube in a plane perpendicular to the axis (identified in green in the center image) is shown to the left, and in a plane parallel to the axis and almost tangential to the nanotube wall (identified in red in the center image) is shown to the right.

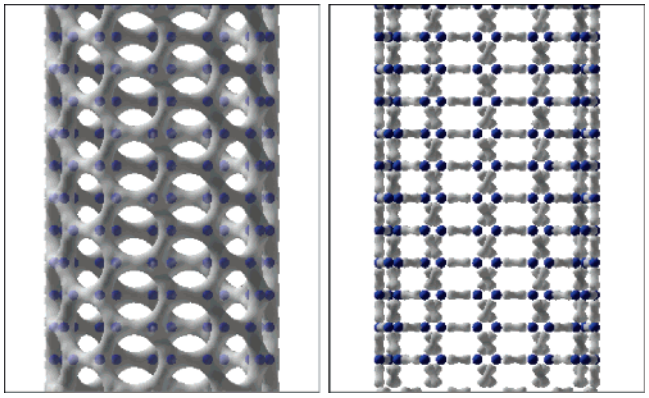

Figure 6. Iso-surface applied at a fraction of 0.7 (left) and 0.9 (right) of the total ECD of a (6,6) nanotube. These surfaces correspond to the total bonding surface and the sp^2 bonding surface, respectively.

An important aspect that is difficult to deduce from Figures 7d and 8d is the possibility of a dangling bond being formed on the nanotube wall when three H atoms are adsorbed in the pyramid-configuration. As a consequence of this configuration, the sp^3 defect formed by each adsorbate intersects at a central C atom. This means that the C atom located at this position is sp^3 hybridized but only 3-fold coordinated. If formed on a nanotube wall, an sp^3 defect containing a dangling bond would (under the right conditions) offer an ideal nucleation site for the formation of diamond nanocrystals.

3.3 Interaction of Carbon with Defective and Pristine Sites. Finally, to test the energetic favorability of the pyramid site, carbon atoms were adsorbed on this position and the absorption energy compared with that obtained for a site on the SWNT far from the H-defect (a pristine position). The adsorption configurations for the carbon atoms on the outer walls of the defective SWNT correspond to those indicated on the graphene sheet in Figure 9. As in Figure 2, the three H atoms (pyramid-configuration) are indicated in dark blue, and the positions of the adsorbed carbon atoms are circled. This comparison was performed for both the (6,6) and (9,0) nanotubes, and the adsorption energy was obtained using the expression

$$E_b = (E_{CNT,H_N} + E_C - E_{CNT,H_N,C}) \qquad (2)$$

where E_{CNT,H_N} is the total energy of the nanotube with H adsorbates, $E_{CNT,H_N,C}$ is the total energy of the nanotube with H and C adsorbates, and E_C is the energy of a free carbon atom.

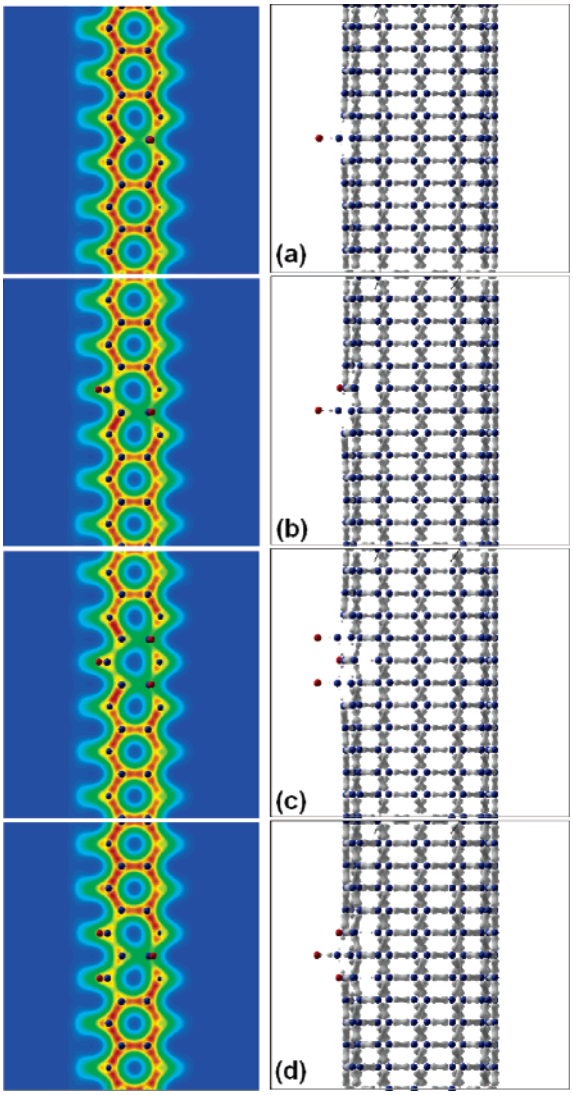

Figure 7. ECD (left) and sp^2 iso-surface (right) for (6,6) SWNT, with (a) one, (b) two, and (c and d) three hydrogen atoms adsorbed to the outer wall. The three H atoms in (c) are adsorbed in the "ring-configuration", and the three H atoms in (d) are adsorbed in the "pyramid-configuration". Carbon atoms are shown in blue and hydrogen atoms are shown in red.

In the case of the pristine position, the adsorption energies for carbon on the (6,6) and (9,0) nanotubes were calculated at −2.18 and −2.93 eV, respectively. In each case however, during the optimization of the structure, the carbon atoms relaxed to a position centered over two neighboring atoms in the tube wall, forming a three-membered ring oriented differently with respect to the tube axis. The C atom adsorbed onto a pristine site of the (6,6) nanotube became centered

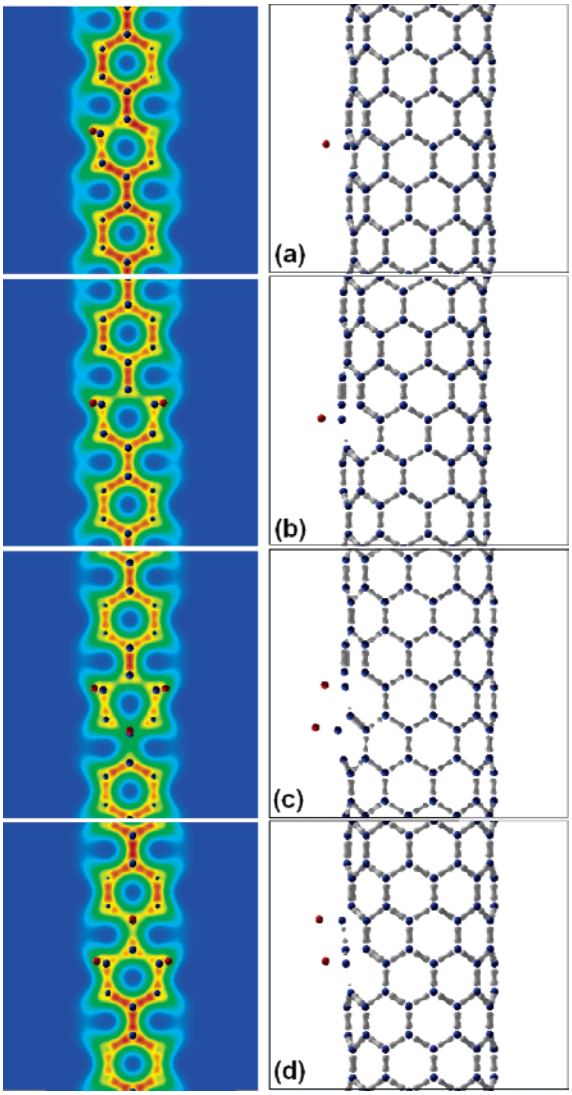

Figure 8. ECD (left) and sp^2 iso surface (right) for (9,0) SWNT, with (a) one, (b) two, and (c and d) three hydrogen atoms adsorbed to the outer wall. The three H atoms in (c) are adsorbed in the "ring-configuration", and the three H atoms in (d) are adsorbed in the "pyramid-configuration". Carbon atoms are shown in blue and hydrogen atoms are shown in red.

over a bond perpendicular to the tube axis, whereas C atom adsorbed onto a pristine site of the (9,0) nanotube became centered over a bond parallel to the tube axis. An example of the (9,0) SWNT is shown in Figure 10a.

This configuration was examined by Krasheninnikov et al,[36] who calculated an adsorption energy of ~2.5 eV for a (9,0) SWNT, also using DFT GGA (PW91) and the PAW potentials. The differences between this result and the value calculated in the current study are attributed to the presence of the extended H-defect on the other side of the nanotube considered herein, which (as mentioned above) distorted the cross-section (and dihedral angles) of the nanotube. As mentioned above this distortion is more pronounced in the (9,0) nanotube, resulting here in a lower C adsorption energy. This distortion appears to have produced more favorable conditions for C adsorption than the ideal nanotubes considered by Krasheninnikov et al.[36]

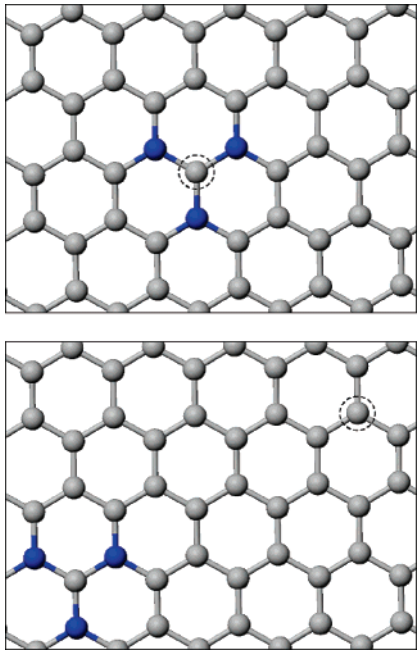

Figure 9. Two adsorption configurations for the carbon atoms on the outer walls of the defective SWNT. The three H atoms in the pyramid-configuration are indicated in dark blue, and the positions of the adsorbed carbon atoms are circled to illustrate the "pyramid" position (top) and "pristine" position (bottom).

In the case of the C adsorption on the pyramid-position, the adsorption energies for carbon on the (6,6) and (9,0) nanotubes were calculated at −3.50 and −4.31 eV, respectively. For both nanotubes, during structural optimization the carbon atoms were found to bind to neighboring H atoms, which then desorbed from the tube wall and formed a C−H group on the surface. The C atom chemisorbed onto the (9,0) nanotube collected one H atom, and the C atom chemisorbed on the (6,6) nanotube collected two H atoms (forming a $C-H_2$ group on the surface). The example of the (9,0) SWNT example is shown in Figure 10b.

In general, although the adsorption on both the pristine and the pyramid sites involved the formation of more than one bond with the adsorbate, the adsorption energies were consistently lower for the pyramid configuration than for the pristine position.

Discussion

Although studies of the adsorption of hydrogen on SWNTs[20,21,34,39] and planar graphene[37] have been undertaken before, such investigations have tended to focus more on the implications of full or partial monolayer coverages, or differences between isotopic species. Hybrid nanocarbons of the type described above[19,18] are characterized by a high nucleation density, but it is the continuous, random impingement of atomic hydrogen that is responsible for the formation of nanoparticle nuclei (rather than the level of coverage), making the local effects of H adsorption important.

(36) Krasheninnikov, A. V.; Nordlund, K.; Lehtinen, P. O.; Foster, A. S.; Ayuela, A.; Nieminen, R. M. *Carbon* **2004**, *42*, 1021.
(37) Ferro, Y.; Marinelli, F.; Allouche, A. *J. Chem. Phys.* **2002**, *116*, 8124.
(38) Zaiser, M.; Banhart, F. *Phys. Rev. Lett.* **1997**, *79*, 3680.
(39) Wang, Q.; Johnson, J. K. *J. Chem. Phys.* **1999**, *110*, 577.

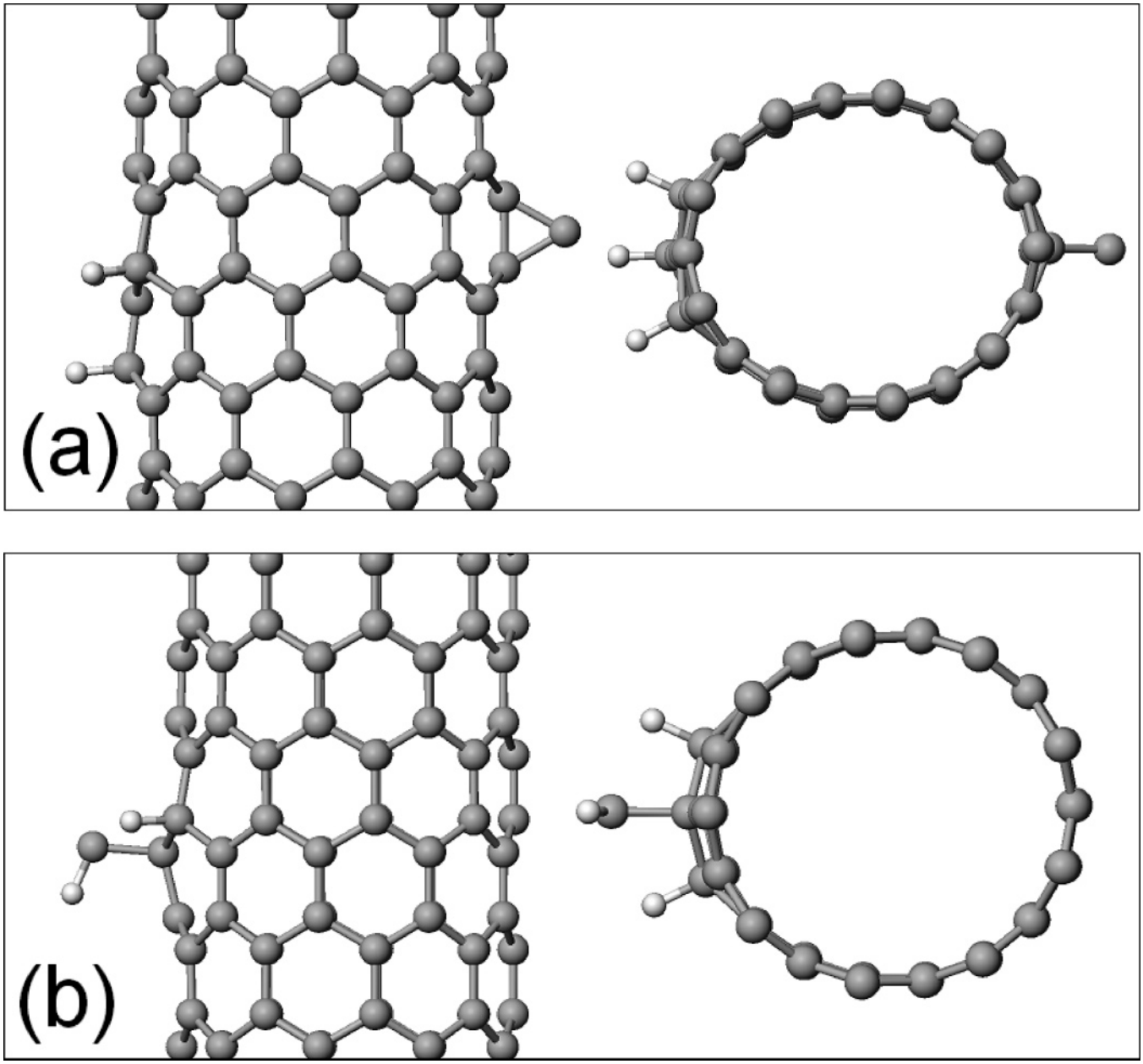

Figure 10. Views perpendicular (left) and parallel (right) to the principal axis of a (9,0) SWNT with three hydrogen atoms and one carbon atom adsorbed to the outer wall. The (a) "pristine" position and (b) "pyramid" position are shown.

The results outlined herein illustrate how finite, isolated sp^3 defect sites may be formed, by comparing various local adsorption configurations. The adsorption configuration (pyramid) that was found to be energetically preferable was also found to contain an under-coordinated sp^3-bonded C atom, which will play an important part in the initiation of diamond nuclei. The addition of more H adsorbates would logically extend the defective region, and increase the probability of dangling sp^3 bonds forming. There are, however, a number of other issues that must be considered, both at the surface and in the center of the hybrid carbon nanomaterials.

One such issue is that of H-etching of the surface of the nanotube substrates. In general, continuous hydrogenation etches sp^2 carbon approximately 10 times faster than sp^3 carbon. This is why etching promotes and stabilizes the sp^3 phase in traditional diamond film deposition. It is likely that etching is also occurring during the formation of 1-dimensional hybrid nanomaterials, promoting a surface supersaturation and localized carbon segregation. The nanotubes become an adjunctive source of carbon species that participate in nanotube growth, and the formation of relief structures.[18] If formed, the summit of such nodules will be active sites for nucleation and subsequent crystallization. Following nucleation and crystallization, the nanodiamond growth may progress in the manner similar to that of diamond chemical vapor deposition processes on amorphous carbon films.[19,18]

Another issue to be considered is that of subsurface phase transitions. The phase transition of carbon-onions into diamond nanoparticles has been know for many years, leading to questions as to why a similar transition can be

avoided during the formation of hybrid nanomaterials such as carbon nanotubes coated with nanodiamond.[18]

The phase transition between nanodiamond and onion-like structures has been previously addressed by Zaiser and Banhart,[38] who presented a thermodynamic quasi-equilibrium theory to explain this irradiation-induced transformation of carbon-onions to nanodiamond. The model was based on the premise that irradiation of carbon-onions leading to the destabilization of the sp^2 structure was due to the large difference in the cross sections for irradiation-induced displacements of carbon atoms in diamond and graphite. A nonequilibrium phase diagram was calculated showing the stability of graphite and diamond (as a function of the displacement rate of atoms), and the results related to the experimentally observed results.[3] In this approach the issue of nucleation was excluded in favor of considering the phase transformation as the motion of a phase boundary separating the two (solid) allotropes. The carbon-onion to nanodiamond phase transition was attributed to ballistic displacements causing interstitial C atoms (predominantly from sp^2 lattice sites) causing a net flux of atoms from the sp^2 to the sp^3 phase. It was shown, however, that if the temperature exceeds an (upper) critical temperature the sp^2 bonding may be stable, even though phase transitions may still occur at lower temperatures.[38]

These findings suggest that although a high substrate temperature is traditionally known to promote nanodiamond formation and stabilization[40] and has been found to assist in the complete conversion of multiwalled nanotubes into nanodiamond,[19] if the temperature is high enough it may also repress the phase transition of sp^2 bonded cores in multi-walled nanotubes or SWNT bundles, thereby allowing hybrid nanostructures the opportunity to develop.

5. Conclusions

In conclusion, the results presented here show that the absorption of atomic hydrogen on the outer walls of SWNTs is successful in creating local, finite sp^3 defects. It has also been shown that, depending upon the adsorption configuration, such defects may contain a dangling bond and thereby produce a site ideal for the nucleation of diamond nanocrystals. This site has been shown to be a low-energy adsorption site for carbon adsorbates than for pristine sites away from the H-induced defect. Although the results show that sp^3 defects are localized around the adsorption sites, and do not extend more than two nearest neighbors from the location C−H bonds, it is possible that the replacement of H atoms with carbon-containing radicals may promote extended defects.

Although a number of important problems remain to be addressed to fully understand the formation and growth of hybrid carbon nanomaterials (such as the kinetic processes at the surface and the structure at the nanotube−nanodiamond interface), it is anticipated that our results will assist in describing the nucleation mechanisms that are known to be critical in the formation of such complicated nanostructures.

Acknowledgment. This work has been partially supported by the U.S. Department of Energy BES-Materials Sciences under contract W-31-109-ENG-38, and by the Italian MIUR through the FIRB National Program. Computational resources for this project have been supplied by Argonne National Laboratory−Laboratory Computing Resource Center, and the Victorian Partnership for Advanced Computing.

CM0488682

(40) Gamarnik, M. Y. *Phys. Rev. B* **1996**, *54*, 2150.